HHS Public Access

Author manuscript

Horm Behav. Author manuscript; available in PMC 2020 February 05.

Published in final edited form as:

Horm Behav. 2019 February ; 108: 20–29. doi:10.1016/j.yhbeh.2018.12.011.

Nanoparticle encapsulation increases the brain penetrance and duration of action of intranasal oxytocin

Aboagyewaah Oppong-Damoah, **Rokon Uz Zaman**, **Martin J. D'Souza**, **Kevin Sean Murnane***

Department of Pharmaceutical Sciences, Mercer University College of Pharmacy, Mercer University Health Sciences Center, Atlanta, GA, USA

Abstract

The blood-brain barrier (BBB) limits the therapeutic use of large molecules as it prevents them from passively entering the brain following administration by conventional routes. It also limits the capacity of researchers to study the role of large molecules in behavior, as it often necessitates intracerebroventricular administration. Oxytocin is a large-molecule neuropeptide with pro-social behavioral effects and therapeutic promise for social-deficit disorders. Although preclinical and clinical studies are using intranasal delivery of oxytocin to improve brain bioavailability, it remains of interest to further improve the brain penetrance and duration of action of oxytocin, even with intranasal administration. In this study, we evaluated a nanoparticle drug-delivery system for oxytocin, designed to increase its brain bioavailability through active transport and increase its duration of action through encapsulation and sustained release. We first evaluated transport of oxytocin-like large molecules in a cell-culture model of the BBB. We then determined *in vivo* brain transport using bioimaging and cerebrospinal fluid analysis in mice. Finally, we determined the pro-social effects of oxytocin (50 μg, intranasal) in two different brain targeting and sustained-release formulations. We found that nanoparticle formulation increased BBB transport both *in vitro* and *in vivo*. Moreover, nanoparticle-encapsulated oxytocin administered intranasally exhibited greater pro-social effects both acutely and 3 days after administration, in comparison to oxytocin alone, in mouse social-interaction experiments. These multimodal data validate this brain targeting and sustained-release formulation of oxytocin, which can now be used in animal models of social-deficit disorders as well as to enhance the brain delivery of other neuropeptides.

Keywords

Nanotechnology; Oxytocin; Social behavior; Bioimaging; Cell culture; Blood-brain barrier; Rabies virus glycoprotein

*Corresponding author at: Department of Pharmaceutical Sciences, Mercer University College of Pharmacy, Mercer University Health Sciences Center, 3001 Mercer University Dr., Atlanta, GA 30341, USA. murnane_ks@mercer.edu (K.S. Murnane).

Disclosure

The authors have no conflicts of interest to disclose.

1. Introduction

Neuropeptides are small protein-like molecules that are commonly co-released with neurotransmitters to modulate neurotransmission. Neuropeptides vary in their size, the neuroanatomical distribution of the neurons in which they are synthesized, and in the neurotransmitters with which they partner for co-release. They have critical roles in behavior and they have shown promise as potential therapeutics for central nervous system (CNS) disorders, because animal studies demonstrate efficacy across a number of disease states (Donaldson and Young, 2008; Engelmann et al., 1996; Klemp and Woldbye, 2001; Reibel et al., 2001; Woldbye, 1998). Unfortunately, their therapeutic potential is limited by the facts that 1) they do not readily cross the blood-brain barrier (BBB) following exogenous administration and 2) their half-lives in the blood are short, typically on the order of minutes. Poor target penetrance and short half-lives are key factors that limit our ability to administer neuropeptides as therapies. Likewise, these factors limit the capacity of preclinical researchers to study the effects of neuropeptides on behavior, as they are often limited to studies using intracerebroventricular administration. The development of a technology that allows for the administration of neuropeptides through less invasive routes of administration may facilitate new discoveries into the role of neuropeptides in behavior and its underlying neural circuitry. As such, in the present study, we characterized a nanoparticle-based formulation designed to increase the brain penetrance and extend the duration of action of neuropeptides.

Although there are many neuropeptides with potential behavioral effects and therapeutic benefits, one of particular interest is oxytocin (OT). OT is a nine-amino acid neuropeptide that is synthesized in the paraventricular and supraoptic nuclei of the hypothalamus. It is released into peripheral circulation by the posterior pituitary gland but also functions as a neurotransmitter, acting at one identified OT receptor, throughout much of the mammalian brain (Carson et al., 2013). Although OT has been traditionally recognized to be involved in uterine stimulation during parturition, recent studies have convincingly demonstrated roles for the brain neurotransmitter OT system in social behavior, social recognition, social comfort, and altruism (Donaldson and Young, 2008; Engelmann et al., 1996; Modi and Young, 2012), which has led to considerable interest in the therapeutic use of OT for CNS disorders with social deficit components, including Autism Spectrum Disorder (ASD), Fragile X syndrome, and Dravet syndrome. Recent work has focused on the use of intranasal delivery to develop OT as a therapeutic (Keech et al., 2018). While promising, this approach has yielded tentative support for the use of intranasal OT, potentially due to its poor bioavailability and brain penetrance even when administered using this route (Keech et al., 2018; Leng and Ludwig, 2016). Likewise, the role of OT in social behavior is complex. A recent study, for example, reported that chronic administration of intranasal OT daily for 30 days in the BTBR mouse model of ASD resulted in minimal effects in dyadic social interactions, three-chambered social approach, open-field exploratory activity, repetitive self-grooming and fear-conditioned learning and memory (Bales et al., 2014). Other studies have shown that the effects of OT on social behavior can depend on factors such as sex, context, age of administration, and dose (Guoynes et al., 2018), can differ between acute and chronic administration (Huang et al., 2014), and chronic OT administration can alter the

expression of OT receptors (Freeman et al., 2018). Much work needs to be completed to fully understand the role of OT in behavior, as well as its potential as a long-term therapeutic. A technology that increases the brain penetrance and sustains the delivery of OT should facilitate these endeavors.

The BBB is a dynamic interface that restricts the movement of most drugs and blood borne molecules into the brain. The tight junctions of the BBB are formed by endothelial cells. Only lipophilic and low molecular weight (< 400 Da) drugs can passively cross the BBB. Therefore, the BBB represents one of the most difficult biological barriers to cross to study the role of large molecules in behavior or to deliver therapeutic agents/drugs/peptides for treatment of CNS diseases (Abbott et al., 2010; Ballabh et al., 2004; Pardridge, 2014). To transport nutrients from blood to brain, the BBB endothelium is equipped with a variety of molecular transport systems. Receptor-mediated transcytosis is a class of transport system that transports macromolecules like insulin and iron between blood and brain. The transferrin (Tf) system is an endogenous iron transport system and many previous studies have attempted to repurpose this endogenous system to target drug formulations to the brain (Broadwell et al., 1996; Gan and Feng, 2010; Pardridge, 2014; Qian et al., 2002; Ulbrich et al., 2009). Tf bound agents cross the BBB (Broadwell et al., 1996; Pardridge, 2014; Qian et al., 2002; Ulbrich et al., 2009) *via* receptor-mediated transcytosis and drug transport across the BBB may be enhanced by Tf conjugated delivery systems as Tf-receptors (TfR) are overexpressed in brain capillary endothelium (Pang et al., 2011; Qian et al., 2002; Ulbrich et al., 2009; Wiley et al., 2013; Yan et al., 2013; Ying et al., 2010). In support of this idea, Pang et al. showed the uptake of Tf polymersomes by BEND3 cells occurs primarily through clathrin mediated energy dependent endocytosis. Also, after tail IV injections there was more brain accumulation of Tf polymersomes than unconjugated polymersomes (Pang et al., 2011). Recent studies, also, have described a new brain targeting ligand called Rabies Virus Glycoprotein (RVG), which putatively binds to nicotinic cholinergic receptors (nAChR) on the BBB to engage brain uptake of drug formulations (Kim et al., 2013; Liu et al., 2016). As both Tf and RVG have been used previously to target therapeutic large molecules to the brain, it is reasonable to expect that they will be effective in the brain transport of neuropeptides. In addition to Tf and RVG, there are a number of other receptor and transporter systems that may allow for the development of novel brain targeting nanoparticle formulations. For example, the P-glycoprotein transporter, excitatory amino acid transporter, dopamine transporter, and nucleoside transporter are expressed in the nasal mucosa (Anand et al., 2014). As such, a wide diversity of drug targeting systems could be developed that take advantage of these endogenous systems. To the best of our knowledge, our work is among the first to apply such an approach to OT and other neuropeptides.

Previous studies have used a variety of approaches for sustained delivery and brain targeting of drug formulations. Molecules can be encapsulated within different polymers including Poly(lactic-*co*-glycolic acid) (PLGA), bovine serum albumin (BSA), polyethyleneglycol, lipopolyplexes, polymer-based cyclodextrin, and gold nanoparticles (Jones et al., 2011; Kolluru et al., 2013; Li et al., 2003; Pan et al., 2008; Sahoo and Labhasetwar, 2005; Zhang et al., 2009). We focused our efforts on BSA nanoparticles, because they are biocompatible and biodegradable (Makadia and Siegel, 2011), we have previously shown low levels of toxicity with these polymers in both cells (Zaman et al., 2018) and nonhuman primates (Oettinger et

al., 2007), and we have not observed any signs of toxicity in mice. Furthermore, we have shown that these polymers have sustained-release properties (Tong et al., 2003).

In the present study, we evaluated a nanoparticle drug-delivery system for OT designed to increase its brain bioavailability through active transport and sustain its delivery through encapsulation and sustained release. We first evaluated transport of OT-like large molecules using our technology in a cell-culture model of the BBB. We then determined *in vivo* brain transport using bioimaging and cerebrospinal fluid (CSF) analysis. Finally, we determined the efficacy of OT in two different brain targeting and sustained-release formulations in a mouse model of social behavior. Our central hypothesis is that this novel drug formulation increases the brain penetrance and sustains the delivery of intranasal OT.

2. Materials and methods

2.1. Drugs/chemicals

Poly(D,L-lactide-*co*-glycolide) lactide:glycolide (50:50), Polyvinyl Alcohol, Dichloromethane and Indocyanine green (ICG) were purchased from Sigma Aldrich (Milwaukee, WI, USA). Bovine serum albumin (Fraction V), glutaraldehyde (25% in water) and acetone were purchased from Fischer Scientific (Pittsburgh, PA, USA). All the chemicals were of analytical grade and used as is without further modification. OT (GenScript USA, Piscataway, NJ) was dissolved in a mixture of 10% Tween-80 and saline and lightly vortexed for suspension. Nanoparticles equivalent to 50 μg of oxytocin was suspended in 50 μl of vehicle for each intranasal administration.

2.2. Preparation of nanoparticles

We recently reported a series of studies to refine and optimize our approach to the preparation of nanoparticles for brain targeting (Zaman et al., 2018). Bovine serum albumin (BSA) nanoparticles were prepared by a coacervation/nanoprecipitation method followed by lyophilization. Briefly, 270 mg of BSA and either 27 mg of OT, 27 mg of FITC or 2.7 mg of ICG (depending on the particular experiment) were dissolved in 10 ml of 10 mM NaCl at pH 9.3. Acetone was added drop wise at a speed of 1 ml/min to the aqueous solution at a ratio of 2:1 with stirring at 800 rpm. After desolvation, the nanoparticle suspension was cross-linked for 24 h with 25% (w/v) glutaraldehyde in water (200 μl of glutaraldehyde for 1000 mg of BSA). Excess of glutaraldehyde was neutralized with sodium bisulphite. Trehalose (2% w/v) was added as a cryoprotectant and the nanoparticle suspension was lyophilized using Labconco freeze dryer (Labconco corporation, Missouri, USA).

2.3. Tf and RVG conjugation to peptide-loaded nanoparticles

Previous studies have used Tf and RVG as brain targeting ligands (Broadwell et al., 1996; Gan and Feng, 2010; Kim et al., 2013; Liu et al., 2016; Pardridge, 2014; Qian et al., 2002; Ulbrich et al., 2009) using other formulation technologies and to carry therapeutics other than neuropeptides into the brain. We attempted to adopt their approaches for nanoparticle formulations of neuropeptides. Tf and RVG were conjugated to BSA nanoparticles in two steps. The first step required activation of the carboxylic acid terminal groups using 1-ethyl-3-(3-dimethylaminopropyl)carbodiimide (EDC) and *N*-Hydroxysulfosuccinimide

(NHS) (98%) followed by conjugating Tf or RVG in the nanoparticles. Briefly, 1 ml (1 mg/ml) of EDC and NHS (1 ml, 1 mg/ml) was added to 10 ml of nanoparticle suspension containing 40 mg of OT-loaded BSA nanoparticles. The nanoparticles were dispersed in 1 ml of PBS, and Tf (1 ml, 1 mg/ml) or RVG (1 ml, 1 mg/ml) was added drop-wise to the mixture. The mixture was stirred at room temperature for 2 h and incubated at 4 °C overnight or 12 h. The samples were washed and lyophilized.

2.4. BEND3 cell culture

To generate a cellular model of the BBB, BEND3 cells were obtained from American Type Culture Collection (ATCC: 2299). BEND3 cells are endothelial cells that form tight barriers through the formation of transcellular tight junctions (Montesano et al., 1990; Sikorski et al., 1993; Williams et al., 1988), and these barriers mimic the barrier properties of the BBB (He et al., 2010; Watanabe et al., 2013). Their endothelial nature has been confirmed by the expression of von Willebrand factor and the uptake of fluorescently labeled low density lipoprotein. BEND3 cells were cultured in Dulbecco's Modified Eagle Medium (DMEM) supplemented with 15% FBS and 1% (100 U/ml Penicillin and 100 μg/ml Streptomycin). The cells were quickly thawed and centrifuged at 250 ×*g* for 8 min in 5 ml of complete media. The cell pellets were resuspended in 1 ml of complete media and plated on T-25 flask. Cells were maintained at 5% CO_2, 37 °C, and 80% humidity in a cell-culture incubator. At confluence, the cells were washed twice with 2.5 ml DPBS, trypsinized with TrypLE and centrifuged at 250 ×*g* for 8 min at 4 °C. The cells were then resuspended in 1 ml of complete media and plated onto T-75 flask at appropriate densities for continuous passaging of the cells.

To characterize the membrane properties of the artificial BBB formed by these cells, the cells were seeded and cultured on permeable transwells using procedures we optimized following the literature (Wuest et al., 2013). Confluent cells from T-75 flasks the cells were washed twice with 4 ml DPBS, trypsinized with TrypLE and centrifuged at 250 ×*g* for 8 min at 4 °C. The cells were then resuspended in 1 ml of complete media. 15 μl of cell suspension was diluted with 15 μl of 0.4 trypan blue solution and a cell count was taken using a Countess II automated cell counting machine (MAN 0014293, Life Technologies, CA). The cells were diluted and seeded onto Costar permeable 12-well collagen coated membrane transwells with a 3 μm pore size (Corning; Corning, NY) a density of 4×10^6 cells/insert in 0.5 ml of complete media. 1.5 ml of complete media was put on the basolateral side of the transwell while 0.5 ml of cell suspension was put into the apical side of the transwell insert. The media on both apical and basolateral sides of the transwell was changed every other day with complete media. All cells used for this work were below passage 33.

2.5. Transepithelial electrical resistance (TEER)

TEER measurements are a precise and well accepted method for assessing the barrier function of *in vitro* membranes prior to drug or formulation transport or barrier integrity studies (Li et al., 2004; Srinivasan et al., 2015). Following plating of the BEND3 cell on the transwells, the confluence of the cellular monolayer was manually monitored daily using microscopy. Furthermore, the resistance of the cellular monolayer was manually monitored daily using a Millicell-ERS-1 Epithelial Volt/Ohm Meter (EVOM Meter: MERS00001;

MilliporeSigma; Burlington, Massachusetts). Briefly, the electrodes are sterilized with 70% ethanol and equilibrated in complete growth media. The resistance of the blank membrane was recorded as well as that of the cells, and the resistance of the blank membrane was subtracted from the resistance of the cell barrier. During resistance measurements, the electrodes are positioned such that the silver-silver chloride pellet neither touches the membrane of the insert nor is exposed to air. Actual voltage readings are obtained by subtracting blank resistance values. An intact monolayer of barrier cells in culture, as occurs when the cells reach confluence, causes an increase in resistance across the membrane, from 5 ohms per cm^2 ($\Omega \cdot cm^2$) to 50–100 $\Omega \cdot cm^2$. This typically was achieved between 6 and 8 days following plating.

2.6. BBB transport

To study the transport of nanoparticle formulations across the BEND3 BBB model barrier, we used a complete Ussing chamber system with a multichannel voltage-current clamp and the EasyMount Ussing chambers (Model VCC MC8; P2300; Physiologic Instruments Inc.; San Diego, CA). The combination of the Ussing chambers and multichannel voltage-current clamp provided an apparatus for determining accurate nanoparticle transport and precise real-time and continuous measurements of the BEND3 membrane barrier function and bioelectric properties – TEER, short circuit current I_{SC}, and potential difference PD. The multiple endpoints allow for a comprehensive evaluation of barrier function. The real-time and continuous access to the data ensure that experiments are only conducted with functional barriers and that administration of the nanoparticles do not disrupt barrier function. This system was used for final experiments once the cultures reached appropriate resistance as verified by EVOM measurements. To subtract the background resistance, a blank cell-culture insert was placed onto the slider and used to compensate for any fluid or blank membrane resistance by dialing off any reading to zero. Voltage differences between the electrodes were also offset. The blank inserts were then replaced with inserts containing cells and kept a temperature of 37 °C throughout the duration of the experiment. The cells were allowed to equilibrate in the Ussing chamber for 15 min before start of the experiment. Before the start of the experiment, all cell barrier preparations were evaluated for resistance properties and current flow using the acquire and analyze software. The resistance values of the cells during the experiment were obtained using the same software. For each experimental set up, 3 chambers contained cells while one was a blank insert.

For visual confirmation of monolayer formation, a solution (0.4%) of the visible dye trypan blue was used. This was our dye of choice because its molecular weight (986.41 g/mol) is comparable to the molecular weight of OT (1006 g/mol). 100 μl of dye solution was put in the left side of each chamber and sampled from the right compartment at times 1, 2, 3 and 4 h following dye administration. The intensity of dye at the various time points were quantified using a BioTek HT synergy spectrophotometer at 540 nm (Model S1AFR BioTek; Winooski, VT). To detect transport of the nanoparticles across the BBB, fluorescein isothiocyanate (FITC) was encapsulated in BSA nanoparticles using identical procedures to OT encapsulation, and was used to characterize transport of Tf-coated nanoparticles across the formed monolayer. 200 μl of nanoparticles solution of concentration 134 μg/ml solution was put in the left side of each chamber and sampled from the right compartment at times 1,

2, 3 and 4 h. The fluorescent intensity of FITC at the various time points was quantified using BioTek fluorescent spectrophotometer at an excitation wavelength of 485 nm and an emission wavelength of 528 nm. The experiment was conducted in a dark environment to prevent fluorescent photobleaching of FITC.

2.7. Animals

Male Swiss-Webster mice (CFW; Charles River Laboratories, Inc.; Wilmington, MA) weighing between 25 and 40 g served as the subjects of the *in vivo* experiments. The mice were housed in groups of 4 in a temperature and humidity controlled room. Animals had access to food (Laboratory Rodent Diet) and water *ad libitum*. Mice were housed in rooms maintained in a 12-hour light/dark cycle. The lights were turned off at 6 pm every evening, and turned back on at 6 am every morning. All animals employed in this study were treated according to protocols evaluated and approved by Institutional Animal Care and Use Committee of Mercer University.

2.8. Bioimaging

On experimental days, animals were administered nanoparticles loaded with Indocyanine green (ICG) (6.7 μg of dye equivalent) intranasally. All mice were imaged at 0.25, 1.5, 3, 6 and 24 h after intranasal administration using a LI-COR Odyssey Bioimager equipped with a MousePOD for *in vivo* imaging (LI-COR Biosciences; Lincoln, NE). The LI-COR Odyssey Bioimager is a non-invasive near infra-red live imaging technique. Anesthesia was induced immediately prior to each imaging time point with isoflurane and maintained with isoflurane throughout the approximately 30 min of imaging. The integrated intensity of ICG dye in the brain at 800 nm was quantified by the bioimager. For both Tf and RVG nanoparticles, > 90% of the dye appeared to be cleared from the brain in 24 h, most likely due to degradation of the dye itself rather than actual clearance of the nanoparticles from the brain. As the peak intensity of ICG dye in the brain was at approximately 2 h for both Tf and RVG nanoparticles, we used the 2 hour time point for the subsequent *in vivo* cerebrospinal fluid (CSF) analysis and acute social behavior experiments. For all *in vivo* experiments, intranasal administration was accomplished in fully conscious mice using the intranasal grip and application by pipette as has been described previously (Hanson et al., 2013).

2.9. Collection of CSF and plasma

Borosilicate glass capillary with filament (BD 100–75-10, Sutter Instrument Inc.) was pulled in the middle over a Bunsen burner. The tip of the flamed glass capillary tubes was trimmed with scissors so that the tapered tip has an inner diameter of approximately 0.5 mm.

On sample collection days, animals were administered a 50 μl solution of OT alone or encapsulated in nanoparticles (containing 50 μg of OT) intranasally and placed in separate cages for 120 min.

CSF samples were collected from the cisterna magna as previously published by (Liu and Duff, 2008) with little modifications. Briefly, the mice were anaesthetized with isoflurane and maintained under anesthesia at a flow rate of 1.5 ml/min during the surgical process. The mice were then placed prone in the stereotaxic instrument in direct contact with a

heating pad with their heads firmly secured. The skin on the head and neck was shaved and the surgical site wiped with 10% povidone iodine followed by 70% ethanol. An incision was made and the muscles under the skin separated by blunt dissection under a dissecting microscope until the dura of the cisterna magna were exposed (a glistening white reverse triangle). The mice were then repositioned so the head formed a near 135° angle to the body. The dura mater was blotted dry with sterile cotton swab and saline. A capillary tube was inserted into the cisterna magna through the dura mater to allow CSF to flow into the glass capillary tube. The CSF was transferred into a premarked 0.6 ml Eppendorf, immediately placed on ice, and transferred into a −20 °C freezer. Any sample contaminated with blood (pink tinge) was discarded. Immediately after CSF collection, blood samples were collected *via* the facial vein for each mouse into K_2EDTA tubes (BD Microtainer 365974) and immediately placed on ice. The mouse was immediately euthanized by carbon dioxide asphyxiation. Blood samples were spun at 4200 rpm for 10 min at 4 °C after which the plasma fraction was collected and stored at −20 °C until analysis. Samples were not stored for > 10 days.

2.10. Enzyme Linked Immunosorbent Assay (ELISA)

All collected CSF and Plasma samples were treated identically and assayed at the same time with the same batch of reagents. All samples were tested using commercially available oxytocin ELISA kit (ADI-900-153A, Enzo Life Sciences, NY) with a detection limit of 15 pg/ml. The assay was performed on unextracted samples according to the protocol provided by the manufacturer. Briefly, seven standards and samples were diluted 1:7 in assay buffer (30ul of plasma or CSF diluted with 220 of assay buffer) and put in appropriate wells. To ensure ELISA kit was working appropriately, quality control metrics such as the total activity (TA), nonspecific binding (NSB), maximum binding (B0) and blank wells were included in the assay as recommended in the assay protocol. After addition of yellow antibody to all wells except for blank, TA and NSB wells, the plate was tapped gently, sealed, and incubated at 4 °C for 20 h. After three washes, blue conjugate was added to TA wells and pNpp substrate solution was immediately added to all wells and incubated at room temperature without shaking for 1 h after which stop solution was added. The optical density was read immediately at 405 nm with correction at 570 nm using BioTek HT synergy spectrophotometer at 540 nm (Model S1AFR BioTek; Winooski, VT). The mean optical density of the blank wells was subtracted from all readings. The intra assay coefficient of variance was < 10%.

2.11. Social behavior

Social-behavior experiments consisted of dyadic social interactions between familiar mice (mice housed in the same home cage). All experiments were conducted in boxes (33 × 25 × 9 cm) large enough to provide for social separation, with ambient lighting dim enough to allow interactions but bright to enable scoring of the videos. The bedding used for all experiments was from the home cages of the animals to prevent novelty-induced hyper-excitability. Experiments were conducted with the room kept at a minimal noise level. All videos were scored by a trained observer. On experimental days, animals were administered a 50 μl solution of OT alone or encapsulated in nanoparticles (containing 50 μg of OT) intranasally and placed in separate cages for 120 min (n = 4–6 pairs per group). Three days

after the acute session, mice were again separated for 120 min just as in the acute session. The mice were then placed in the testing box, allowed to acclimatize in the box for 5 min and video recorded for 10 min. Behavior was rated on a 6-point scale, composed of: adjacent lying, anogenital sniffing, general investigation, body crossing, aggression, and no social interaction, as has been done previously (Curry et al., 2018). The 50 μg dose of OT was based on preliminary social-behavior experiments. Both animals in the dyadic social interactions were dosed with the OT.

2.12. Data analysis

All graphical data presentations and analyses were completed using GraphPad Prism (GraphPad Software Inc., La Jolla, CA, USA). The cell culture data were analyzed by two-way analysis of variance (ANOVA). Bonferroni post-hoc analyses test was utilized to maintain the probability of making a type 1 error at 5%. The *in vivo* bioimaging data were analyzed by one-way ANOVA followed by Dunnett's post-hoc test as the treatments underwent planned comparisons to a single control group. CSF concentrations of OT were assessed by unpaired *t*-test (Dunnett, 1955). The *in vivo* social behavior and plasma OT levels were analyzed by one-way ANOVA followed by Tukey's post-hoc test as comparisons were made between all treatments (Tukey, 1949). We have routinely used similar analysis in mouse models (Murphy and Murnane, 2018; Ray et al., 2018). Effect sizes were determined by Eta^2 for ANOVA results and Cohen's d for all pair-wise comparisons.

3. Results

3.1. Trypan blue validation study

The integrity of the artificial BBB barrier was assessed using trypan blue transport. The resistance of the cellular barrier (BEND3 cells) at the first sampling point (t = 60 min) was R_t 123.7 ± 54 Ω·cm^2 n = 3 and at t = 240 min was R_t 117.2 ± 42.5 Ω·cm^2; n = 3. The resistance when there was no cellular barrier at t = 60 min was R_t 2.89 + 1.2 Ω·cm^2 n = 3 and at t = 240 min was R_t 4.2 ± 2.7 Ω·cm^2 n = 15. These data indicate that the addition of the trypan blue did not disrupt the cellular barrier.

The transport of trypan blue across the cell barrier was (Fig. 1) assessed by determining the main effect of the presence or absence of the cell barrier and the main effect of time by two-way ANOVA. There was a significant main effect of the presence of the cell barrier ($F_{1,16}$ = 6762; $p < 0.0001$). There was a significant main effect of time ($F_{3,16}$ = 952.1; $p < 0.0001$). There was also a significant interaction ($F_{3,16}$ = 520.2; $p < 0.0001$). Post-hoc analysis revealed significant (t = 13.02, 35.38, 48.93, and 67.14) reductions of trypan blue passage across the cell barrier at 1, 2, 3 and 4 h. The effect sizes (Eta^2) for these main effects and this interaction were 0.60, 0.26, and 0.14, respectively. There was significant reduction in the transport of trypan blue in the presence of the cell barrier at all time points ($p < 0.001$ at all time points).

3.2. FITC transport

Transport of FITC in brain targeting nanoparticles across the artificial BBB barrier (Fig. 2) was assessed by determining the main effect of the presence or absence of the cell barrier

and the main effect of time by two-way ANOVA. There was no significant main effect of the barrier ($F_{1,16} = 0.79$; $p < 0.3844$). There was a significant main effect of time ($F_{3,16} = 16.90$; $p < 0.0001$). The effect size (Eta^2) for this main effect was 0.73. There was no significant interaction between these factors ($F_{3,16} = 0.7816$; $p < 0.5214$). Post-hoc analysis revealed (t = 0.7860, 0.8593, 0.7654, 1.097) no significant differences due to the presence of the cellular barrier at any time point. There were no significant differences in transport of FITC in brain targeting nanoparticles due to the presence or absence of the cell barrier, indicating that the brain targeting particles rapidly surmount the barrier, most likely through active transport across this barrier. The resistance of the cellular barrier (BEND3 cells) at the first sampling point (t = 60 min) was R_t 107.28 ± 31.7 $\Omega \cdot cm^2$ (n = 5), and at the end of the experiment (t = 240 min), it was R_t 127.22 ± 28 $\Omega \cdot cm^2$ (n = 5). Without the cellular barrier, the resistance of the cellular barrier at the first sampling point (t = 60 min) was R_t 5.03 + 1.8 $\Omega \cdot cm^2$ (n = 5), and at the end of the experiment (t = 240 min), it was t = 240 min R_t 10.8 ± 2 $\Omega \cdot cm^2$ (n = 5).

3.3. Bioimaging

The time course of brain uptake of ICG alone or ICG in each of the two formulations was determined. The area under the curve (AUC) of the time course in each animal was determined and tabulated for statistical analyses. One-way ANOVA revealed a significant main effect of treatment ($F_{2,12} = 5.098$; $p < 0.0250$) on brain penetrance of ICG nanoparticles (Fig. 3). The effect size (Eta^2) for this main effect was 0.46. Post-hoc analysis by Dunnett's test revealed that OT in RVG-conjugated nanoparticles (q = 2.960) at a concentration of 6.7 μg and OT in Tf-conjugated nanoparticles (q = 2.518) at a concentration of 6.7 μg were significantly different from ICG solution group.

3.4. Plasma and CSF analysis

Consistent with the bioimaging data, 2 h after intranasal administration, we observed significantly higher levels of OT in CSF ($t = 7.501$; $p < 0.05$) when it was administered in RVG-conjugated nanoparticles compared to when it was administered alone (Fig. 4, TOP). The effect size (Cohen's d) for this was 11.00. This comparison was only made for OT treatments as the CSF levels of OT were below the limit of detection following vehicle treatment. For the plasma analysis, the vehicle treatment showed a detectable level of OT. One-way ANOVA revealed a significant main effect of treatment ($F_{2,5} = 14.35$; $p < 0.05$) on plasma levels of OT (Fig. 4, BOTTOM). The effect size (Eta^2) for this main effect was 0.91. Post-hoc analysis by Tukey's test revealed that intranasal administration of free OT resulted in significantly higher levels of OT (q = 7.568) in plasma compared vehicle treatment. There was no significant difference in plasma CSF levels between vehicle treatment and administration of OT in RVG-conjugated nanoparticles (q = 3.487) or between administration of free OT or OT in RVG-conjugated nanoparticles (q = 4.081) Nanoparticle encapsulation resulted in a significant increase in CSF levels of OT, in the absence of a significant increase in plasma levels. It is important to note, however, that there remains some OT that continues to make it to the plasma even with nanoparticle encapsulation, especially when one considers the larger volume of distribution in plasma compared to CSF.

3.5. Social behavior

One-way ANOVA revealed a significant main effect of treatment ($F_{3,32} = 8.897$; $p < 0.0002$) on murine social interactions (Fig. 5, TOP). The effect size (Eta^2) for this main effect was 0.45. Post-hoc analysis by Tukey's test revealed that OT in RVG-conjugated nanoparticles ($q = 4.530$) or Tf-conjugated nanoparticles ($q = 6.182$) at a concentration of 50 μg was significantly different from vehicle. Post-hoc analysis also showed that OT in Tf-conjugated nanoparticles ($q = 5.317$) was significantly different from 50 μg of OT alone. One-way ANOVA of social behavior 3 days after treatment revealed a significant main effect ($F_{3,32} = 8.897$; $p < 0.0001$) of treatment on overall social interactions (Fig. 5, BOTTOM). The effect size (Eta^2) for this main effect was 0.74. Post-hoc analysis by Tukey's test revealed that OT in RVG-conjugated nanoparticles ($q = 8.757$) or Tf-conjugated nanoparticles ($q = 10.14$) was significantly different from vehicle. Moreover, OT in RVG-conjugated nanoparticles ($q = 8.871$) or Tf-conjugated nanoparticles ($q = 10.27$) was significantly different from OT alone. General Investigation has been previously reported to be the dominant social parameter (Curry et al., 2018) when mice are given the highly prosocial and brain penetrant small molecule 3,4-methylenedioxymethamphetamine (MDMA) (Dumont et al., 2009), which is known to release OT (Harris et al., 2002; Murnane et al., 2010; Murnane et al., 2012; Thompson et al., 2007). Consistent with those data, the dominant social behavior in our mice was general investigation both after acute administration of nanoparticle encapsulated OT and 3 days later. One-way ANOVA revealed a significant main effect ($F_{3,32} = 4.336$; $p < 0.0113$) of treatment on general investigation following acute treatment (Fig. 6, TOP). The effect size (Eta^2) for this main effect was 0.29. Post-hoc analysis Tukey's test revealed that OT in RVG-conjugated nanoparticles ($q = 4.460$) was significantly different from vehicle. OT in RVG-conjugated nanoparticles ($q = 4.043$) was significantly different from OT in Tf-conjugated nanoparticles. After 3 days, there was a significant main effect of treatment ($F_{3,32} = 43.84$; $p < 0.0006$) on general investigation (Fig. 6, BOTTOM). The effect size (Eta^2) for this main effect was 0.80. Post-hoc analysis revealed that OT in RVG-conjugated nanoparticles ($q = 10.41$) or Tf-conjugated nanoparticles ($q = 12.91$) was significantly different from vehicle. Also, OT in RVG-conjugated nanoparticles ($q = 9.575$) or Tf-conjugated nanoparticles ($q = 12.00$) was significantly different from OT alone.

4. Discussion

In the present study, we evaluated transport of OT-like large molecules using our functionalized nanoparticle technology in a cell-culture model of the BBB and *in vivo* using bioimaging. We determined the efficacy of OT in two different brain targeting and sustained-release formulations in a mouse model of social behavior. We found that our nanoparticle formulation increases BBB transport both *in vitro* and *in vivo*. Moreover, nanoparticle-encapsulated OT administered intranasally exhibited greater pro-social effects both acutely and 3 days after administration relative to OT alone. Both Tf and RVG nanoparticles produced robust acute and sustained elevations in overall social behavior that were comparable in their magnitude to each other. These acute prosocial effects were also in near agreement in their magnitude to those of MDMA in mice (Curry et al., 2018) and MDMA in rats (Morley et al., 2005; Thompson et al., 2007), which is a strongly prosocial and brain penetrant small molecule that elicits release of OT (Harris et al., 2002; Murnane et al., 2010;

Murnane et al., 2012; Thompson et al., 2007). Interestingly, the two different brain targeting ligands differed in the nature of the pro-social effects that they elicited, with RVG selectively increasing general investigation and Tf increasing a mixed response of general investigation in some subjects and adjacent lying (data not shown) in other subjects with acute administration. Previous studies have shown that acute MDMA administration selectively increases general investigation in mice (Curry et al., 2018) but has more of a mixed response between general investigation and adjacent lying in rats (Morley et al., 2005; Thompson et al., 2007). It is important to note that both animals in the dyadic social interactions were dosed with the OT. This makes it difficult to elucidate the mechanisms through which OT is changing social behavior. However, this approach was chosen to establish the proof of principle that this technology is effective. Furthermore, it should also be recognized that the same animal was assessed repeatedly in the social behavior experiments. As such, it is possible that the acute administration of OT led to persistent changes in the brain or that the experience itself led to persistent increases in social behavior, in contrast to the hypothesis that the OT remained functional after 3 days. Studies consistent with this possibility have been reported recently (Price et al., 2017; Rilling et al., 2017). We are now prepared to tackle such issues as this proof of principle study allows for nanoparticle encapsulation to be applied in future studies to rigorously study the role of OT in social behavior, other behaviors, and other CNS-mediated effects.

It is possible that any observed differences between the RVG and Tf brain targeting ligands may be due to the kinetics of brain transport or the kinetics of release of OT from BSA conjugated to these ligands. This is particularly true for formulations that are delivered intranasally as Tf receptors are highly expressed on nasal mucosa, and enhanced transport across the nasal mucosa may provide access to the BBB, which also expressed Tf receptors. For example, a previous study showed that conjugation of Tf to a model HIV antigen allows Tf to retain its high affinity for its receptor, that the conjugate was specifically transported across the nasal mucosal epithelial barrier, and that it achieves significantly higher and robust antibody titer levels compared to the unconjugated antigen (Mann et al., 2012). Likewise, transportation, transfection efficiency, and growth factor inhibition were tested in the bovine nasal epithelia using several formulations of an anti-vascular endothelial growth factor interceptor plasmid, and supporting the use of PLGA and Tf conjugation, it was reported across all measures that the rank order of effectiveness was as follows for various nanoparticle formulations: Tf-PLGA > deslorelin-PLGA > PLGA ≫ plasmid alone (Sundaram et al., 2009). In conjunction with the literature demonstrating the viability of Tf as a brain targeting ligand, these data specific to the nasal epithelium provide particular support for its use for intranasal delivery. RVG, on the other hand putatively binds to nAChRs on the BBB to engage brain uptake of drug formulations (Kim et al., 2013; Liu et al., 2016). Reverse transcription-PCR has shown that several non-neuronal nAChR subunits are expressed in the nasal mucosa, including alpha and beta subunits (Keiger et al., 2003). There is evidence that nAChRs are expressed at significant densities on nasal trigeminal nerve endings of the rat, suggesting an anatomical distribution of these receptors that may facilitate direct bypass of the BBB (Alimohammadi and Silver, 2000). Intranasal inoculation of the rabies virus is believed to allow the virus to directly access the brain *via* the olfactory epithelium, either along the olfactory nerve or the trigeminal nerve (Lafay et al., 1991;

Terryn et al., 2014). It is also possible that differences in behavioral outcomes between these two brain targeting ligands may be mediated by differential pharmacokinetics in the release profile from the particle matrix. BSA is biodegradable and as its polymer shell is degraded in a biological matrix the OT gets released in a controlled manner, upon which it is now free to act upon its receptor targets. The glutaraldehyde crosslinking slows down the rate of degradation. We have determined *in vitro* using a plasma matrix that release from BSA particles does vary based on whether they are conjugated to RVG or Tf (Zaman et al., 2018), but it remains to be determined whether this varies *in vivo*.

Drugs have been administered through the intranasal route of administration for millennia. However, interest in intranasal drug delivery has been growing in recent years, particularly with the promise of intranasal OT for ASD. Intranasal delivery is particularly favorable when adverse or other factors limit oral dose delivery or when increased brain penetrance is desirable. Possible mechanisms through which intranasally delivered OT gets to the brain include a direct access *via* extraneuronal/perineuronal routes along the trigeminal or olfactory nerve pathway. This route not only gives access to the CSF but also hippocampus and amygdala (Chen et al., 1998), which are rich in oxytocin receptors (Gimpl and Fahrenholz, 2001; Lin et al., 2017; Zoicas et al., 2014). Extraneuronal/perineuronal transport may be particularly useful for RVG nanoparticles as OT released after biodegradation of the BSA polymer shell will have immediate access to oxytocin receptors and the RVG may enhance delivery along these routes. In addition to receptor-mediated transcytosis, other mechanisms that could possibly provide for rapid brain penetrance following intranasal delivery include bulk flow, lymphatic channel, interneuronal transport and active or passive transport from vasculature. Furthermore, it is possible that some of the central effects of intranasally administered OT may be due to stimulation of endogenous OT system in addition to availability of OT within the brain.

The development of intranasal OT delivery is a significant advance in the field of ASD research. Our intention is not to downplay or replace this advance. We hope that our formulation strategy will support the development of intranasal OT therapy, and allow it to fulfill its promise. A significant body of research reports key limitations with the intranasal delivery of OT alone (Leng and Ludwig, 2016). It is well known that OT is rapidly metabolized in both blood and cerebrospinal fluid (CSF). OT activates a plethora of systems in the periphery, most notably in the uterus, but in other organ systems as well. It is therefore important that intranasal OT should achieve the best possible ratio of brain to blood levels. Previous work in rodents, primates, and humans indicates that the doses required to achieve brain penetration may induce supraphysiological effects in the periphery (Born et al., 2002; Dal Monte et al., 2014; Leng and Ludwig, 2016; Modi et al., 2014; Robertson et al., 1970; Striepens et al., 2013). This problem may not be addressable without a brain penetrance enhancer, as based on these studies, the calculated maximum transfer of a dose of OT to the brain within 1 h of intranasal delivery is 0.005% (Leng and Ludwig, 2016). Our nanoparticle delivery system provides at least two significant advantages over intranasal delivery of OT alone. 1) It sustains the release of the peptide and therefore likely limits the potential for repeated bolus activation of peripheral systems following the frequent dosing that would likely be required for intranasal OT in the absence of a sustained release formulation. 2) It targets a greater proportion of the OT to the brain, both during the initial application and

during any subsequent passes in the blood circulation that contacts the BBB, which increases the proportion in the brain relative to the periphery and may reduce the required dose.

It is important to note that blood measures of OT have undergone considerably scrutiny and controversy, particular when determined from unextracted samples as we did in the present study (McCullough et al., 2013), and when they are used as a biomarker for central levels (Lefevre et al., 2017). Our data are in agreement with this assertion as nanoparticle encapsulation differentially modified OT levels in the peripheral and central compartments. It is therefore important that we measured the central compartment and found significant elevations in OT in the CSF. Our *in vitro* and *in vivo* data support these contentions and will allow us now test the therapeutic potential of this technology in specific disease-state animal models. However, more studies have to be done to ascertain the effects of OT using our delivery system in both males and females as well as its effects when delivered chronically. Notwithstanding this caveat, the multimodal data presented in this study strongly support the use of our approach to developing a brain targeting and sustained-release formulation of OT. This formulation can now be used to support intranasal delivery of OT and potentially other neuropeptides for both therapeutic endpoints as well as the rigorous study of behavior.

Acknowledgments

These studies represent partial fulfillment of AOs PhD dissertation research project at Mercer University. The authors would like to thank Cherilyn D'Souza for her expert assistance in cell culture and project management.

Funding

This work was supported by the National Institutes of Health [NS100512 (KSM)], the American Epilepsy Society, and the Mercer University College of Pharmacy.

References

Abbott NJ, Patabendige AA, Dolman DE, Yusof SR, Begley DJ, 2010 Structure and function of the blood-brain barrier. Neurobiol. Dis 37, 13–25. [PubMed: 19664713]

Alimohammadi H, Silver WL, 2000 Evidence for nicotinic acetylcholine receptors on nasal trigeminal nerve endings of the rat. Chem. Senses 25, 61–66. [PubMed: 10667995]

Anand U, Parikh A, Ugwu MC, Agu RU, 2014 Drug transporters in the nasal epithelium: an overview of strategies in targeted drug delivery. Future Med. Chem 6, 1381–1397. [PubMed: 25329195]

Bales KL, Solomon M, Jacob S, Crawley JN, Silverman JL, Larke RH, Sahagun E, Puhger KR, Pride MC, Mendoza SP, 2014 Long-term exposure to intranasal oxytocin in a mouse autism model. Transl. Psychiatry 4, e480. [PubMed: 25386957]

Ballabh P, Braun A, Nedergaard M, 2004 The blood-brain barrier: an overview: structure, regulation, and clinical implications. Neurobiol. Dis 16, 1–13. [PubMed: 15207256]

Born J, Lange T, Kern W, McGregor GP, Bickel U, Fehm HL, 2002 Sniffing neuropeptides: a transnasal approach to the human brain. Nat. Neurosci 5, 514–516. [PubMed: 11992114]

Broadwell RD, Baker-Cairns BJ, Friden PM, Oliver C, Villegas JC, 1996 Transcytosis of protein through the mammalian cerebral epithelium and endothelium. III. Receptor-mediated transcytosis through the blood-brain barrier of blood-borne transferrin and antibody against the transferrin receptor. Exp. Neurol 142, 47–65. [PubMed: 8912898]

Carson DS, Guastella AJ, Taylor ER, McGregor IS, 2013 A brief history of oxytocin and its role in modulating psychostimulant effects. J. Psychopharmacol 27, 231–247. [PubMed: 23348754]

Chen XQ, Fawcett JR, Rahman YE, Ala TA, Frey IW, 1998 Delivery of nerve growth factor to the brain via the olfactory pathway. J. Alzheimers Dis 1, 35–44. [PubMed: 12214010]

Curry DW, Young MB, Tran AN, Daoud GE, Howell LL, 2018 Separating the agony from ecstasy: R(−)-3,4-methylenedioxymethamphetamine has prosocial and therapeutic-like effects without signs of neurotoxicity in mice. Neuropharmacology 128, 196–206. [PubMed: 28993129]

Dal Monte O, Noble PL, Turchi J, Cummins A, Averbeck BB, 2014 CSF and blood oxytocin concentration changes following intranasal delivery in macaque. PLoS One 9, e103677. [PubMed: 25133536]

Donaldson ZR, Young LJ, 2008 Oxytocin, vasopressin, and the neurogenetics of sociality. Science (New York, N.Y.) 322, 900–904.

Dumont GJ, Sweep FC, van der Steen R, Hermsen R, Donders AR, Touw DJ, van Gerven JM, Buitelaar JK, Verkes RJ, 2009 Increased oxytocin concentrations and prosocial feelings in humans after ecstasy (3,4-methylenedioxymethamphetamine) administration. Soc. Neurosci 4, 359–366. [PubMed: 19562632]

Dunnett CW, 1955 A multiple comparison procedure for comparing several treatments with a control. J. Am. Stat. Assoc 50, 1096–1121.

Engelmann M, Wotjak CT, Neumann I, Ludwig M, Landgraf R, 1996 Behavioral consequences of intracerebral vasopressin and oxytocin: focus on learning and memory. Neurosci. Biobehav. Rev 20, 341–358. [PubMed: 8880728]

Freeman SM, Ngo J, Singh B, Masnaghetti M, Bales KL, Blevins JE, 2018 Effects of chronic oxytocin administration and diet composition on oxytocin and vasopressin 1a receptor binding in the rat brain. Neuroscience (EPub prior to print).

Gan CW, Feng SS, 2010 Transferrin-conjugated nanoparticles of poly(lactide)-D-alpha-tocopheryl polyethylene glycol succinate diblock copolymer for targeted drug delivery across the blood-brain barrier. Biomaterials 31, 7748–7757. [PubMed: 20673685]

Gimpl G, Fahrenholz F, 2001 The oxytocin receptor system: structure, function, and regulation. Physiol. Rev 81, 629–683. [PubMed: 11274341]

Guoynes CD, Simmons TC, Downing GM, Jacob S, Solomon M, Bales KL, 2018 Chronic intranasal oxytocin has dose-dependent effects on central oxytocin and vasopressin systems in prairie voles (Microtus ochrogaster). Neuroscience 369, 292–302. [PubMed: 29183825]

Hanson LR, Fine JM, Svitak AL, Faltesek KA, 2013 Intranasal administration of CNS therapeutics to awake mice. J. Vis. Exp.(74). 10.3791/4440.

Harris DS, Baggott M, Mendelson JH, Mendelson JE, Jones RT, 2002 Subjective and hormonal effects of 3,4-methylenedioxymethamphetamine (MDMA) in humans. Psychopharmacology 162, 396–405. [PubMed: 12172693]

He F, Yin F, Peng J, Li KZ, Wu LW, Deng XL, 2010 Immortalized mouse brain endothelial cell line Bend.3 displays the comparative barrier characteristics as the primary brain microvascular endothelial cells. Zhongguo dang dai er ke za zhi = Chin. J. Contemp. Pediatr 12, 474–478.

Huang H, Michetti C, Busnelli M, Manago F, Sannino S, Scheggia D, Giancardo L, Sona D, Murino V, Chini B, Scattoni ML, Papaleo F, 2014 Chronic and acute intranasal oxytocin produce divergent social effects in mice. Neuropsychopharmacology 39, 1102–1114. [PubMed: 24190025]

Jones AK, Bejugam NK, Nettey H, Addo R, D'Souza MJ, 2011 Spray-dried doxorubicin-albumin microparticulate systems for treatment of multidrug resistant melanomas. J. Drug Target 19, 427–433. [PubMed: 20678033]

Keech B, Crowe S, Hocking DR, 2018 Intranasal oxytocin, social cognition and neurodevelopmental disorders: a meta-analysis. Psychoneuroendocrinology 87, 9–19. [PubMed: 29032324]

Keiger CJ, Case LD, Kendal-Reed M, Jones KR, Drake AF, Walker JC, 2003 Nicotinic cholinergic receptor expression in the human nasal mucosa. Ann. Otol. Rhinol. Laryngol 112, 77–84. [PubMed: 12537063]

Kim JY, Choi WI, Kim YH, Tae G, 2013 Brain-targeted delivery of protein using chitosan- and RVG peptide-conjugated, pluronic-based nano-carrier. Biomaterials 34, 1170–1178. [PubMed: 23122677]

Klemp K, Woldbye DP, 2001 Repeated inhibitory effects of NPY on hippocampal CA3 seizures and wet dog shakes. Peptides 22, 523–527. [PubMed: 11287110]

Kolluru LP, Rizvi SA, D'Souza M, D'Souza MJ, 2013 Formulation development of albumin based theragnostic nanoparticles as a potential delivery system for tumor targeting. J. Drug Target 21, 77–86. [PubMed: 23036042]

Lafay F, Coulon P, Astic L, Saucier D, Riche D, Holley A, Flamand A, 1991 Spread of the CVS strain of rabies virus and of the avirulent mutant AvO1 along the olfactory pathways of the mouse after intranasal inoculation. Virology 183, 320–330. [PubMed: 2053286]

Lefevre A, Mottolese R, Dirheimer M, Mottolese C, Duhamel JR, Sirigu A, 2017 A comparison of methods to measure central and peripheral oxytocin concentrations in human and non-human primates. Sci. Rep 7, 17222. [PubMed: 29222505]

Leng G, Ludwig M, 2016 Intranasal oxytocin: myths and delusions. Biol. Psychiatry 79, 243–250. [PubMed: 26049207]

Li Y, Ogris M, Wagner E, Pelisek J, Ruffer M, 2003 Nanoparticles bearing polyethyleneglycol-coupled transferrin as gene carriers: preparation and in vitro evaluation. Int. J. Pharm 259, 93–101. [PubMed: 12787639]

Li H, Sheppard DN, Hug MJ, 2004 Transepithelial electrical measurements with the Ussing chamber. J. Cyst. Fibros 3 (Suppl. 2), 123–126. [PubMed: 15463943]

Lin YT, Chen CC, Huang CC, Nishimori K, Hsu KS, 2017 Oxytocin stimulates hippocampal neurogenesis via oxytocin receptor expressed in CA3 pyramidal neurons. Nat. Commun 8, 537. [PubMed: 28912554]

Liu L, Duff K, 2008 A technique for serial collection of cerebrospinal fluid from the cisterna magna in mouse. J. Vis. Exp

Liu Y, An S, Li J, Kuang Y, He X, Guo Y, Ma H, Zhang Y, Ji B, Jiang C, 2016 Brain-targeted co-delivery of therapeutic gene and peptide by multifunctional nanoparticles in Alzheimer's disease mice. Biomaterials 80, 33–45. [PubMed: 26706474]

Makadia HK, Siegel SJ, 2011 Poly lactic-co-glycolic acid (PLGA) as biodegradable controlled drug delivery carrier. Polymers 3, 1377–1397. [PubMed: 22577513]

Mann JF, Stieh D, Klein K, de Stegmann DS, Cranage MP, Shattock RJ, McKay PF, 2012 Transferrin conjugation confers mucosal molecular targeting to a model HIV-1 trimeric gp140 vaccine antigen. J. Control. Release 158, 240–249. [PubMed: 22119743]

McCullough ME, Churchland PS, Mendez AJ, 2013 Problems with measuring peripheral oxytocin: can the data on oxytocin and human behavior be trusted? Neurosci. Biobehav. Rev 37, 1485–1492. [PubMed: 23665533]

Modi ME, Young LJ, 2012 The oxytocin system in drug discovery for autism: animal models and novel therapeutic strategies. Horm. Behav 61, 340–350. [PubMed: 22206823]

Modi ME, Connor-Stroud F, Landgraf R, Young LJ, Parr LA, 2014 Aerosolized oxytocin increases cerebrospinal fluid oxytocin in rhesus macaques. Psychoneuroendocrinology 45, 49–57. [PubMed: 24845176]

Montesano R, Pepper MS, Mohle-Steinlein U, Risau W, Wagner EF, Orci L, 1990 Increased proteolytic activity is responsible for the aberrant morphogenetic behavior of endothelial cells expressing the middle T oncogene. Cell 62, 435–445. [PubMed: 2379237]

Morley KC, Arnold JC, McGregor IS, 2005 Serotonin (1A) receptor involvement in acute 3,4-methylenedioxymethamphetamine (MDMA) facilitation of social interaction in the rat. Prog. Neuro-Psychopharmacol. Biol. Psychiatry 29, 648–657.

Murnane KS, Fantegrossi WE, Godfrey JR, Banks ML, Howell LL, 2010 Endocrine and neurochemical effects of 3,4-methylenedioxymethamphetamine and its stereoisomers in rhesus monkeys. J. Pharmacol. Exp. Ther 334, 642–650. [PubMed: 20466795]

Murnane KS, Kimmel HL, Rice KC, Howell LL, 2012 The neuropharmacology of prolactin secretion elicited by 3,4-methylenedioxymethamphetamine ("ecstasy"): a concurrent microdialysis and plasma analysis study. Horm. Behav 61, 181–190. [PubMed: 22197270]

Murphy TJ, Murnane KS, 2018 The serotonin 2C receptor agonist WAY-163909 attenuates ketamine-induced hypothermia in mice. Eur. J. Pharmacol 842, 255–261. [PubMed: 30412729]

Oettinger CW, D'Souza MJ, Akhavein N, Peer GT, Taylor FB, Kinasewitz GT, 2007 Pro-inflammatory cytokine inhibition in the primate using microencapsulated antisense oligomers to NF-kappaB. J. Microencapsul 24, 337–348. [PubMed: 17497387]

Pan X, Guan J, Yoo JW, Epstein AJ, Lee LJ, Lee RJ, 2008 Cationic lipid-coated magnetic nanoparticles associated with transferrin for gene delivery. Int. J. Pharm 358, 263–270. [PubMed: 18384982]

Pang Z, Gao H, Yu Y, Guo L, Chen J, Pan S, Ren J, Wen Z, Jiang X, 2011 Enhanced intracellular delivery and chemotherapy for glioma rats by transferrin-conjugated biodegradable polymersomes loaded with doxorubicin. Bioconjug. Chem 22, 1171–1180. [PubMed: 21528923]

Pardridge WM, 2014 Blood-brain barrier drug delivery of IgG fusion proteins with a transferrin receptor monoclonal antibody. Expert Opin. Drug Deliv 1–16.

Price D, Burris D, Cloutier A, Thompson CB, Rilling JK, Thompson RR, 2017 Dose-dependent and lasting influences of intranasal vasopressin on face processing in men. Front. Endocrinol 8, 220.

Qian ZM, Li H, Sun H, Ho K, 2002 Targeted drug delivery via the transferrin receptor-mediated endocytosis pathway. Pharmacol. Rev 54, 561–587. [PubMed: 12429868]

Ray A, Chitre NM, Daphney CM, Blough BE, Canal CE, Murnane KS, 2018 Effects of the second-generation “bath salt” cathinone alpha-pyrrolidinopropiophenone (alpha-PPP) on behavior and monoamine neurochemistry in male mice. Psychopharmacology (EPub ahead of print).

Reibel S, Nadi S, Benmaamar R, Larmet Y, Carnahan J, Marescaux C, Depaulis A, 2001 Neuropeptide Y and epilepsy: varying effects according to seizure type and receptor activation. Peptides 22, 529–539. [PubMed: 11287111]

Rilling JK, Li T, Chen X, Gautam P, Haroon E, Thompson RR, 2017 Arginine vasopressin effects on subjective judgments and neural responses to same and othersex faces in men and women. Front. Endocrinol 8, 200.

Robertson GL, Klein LA, Roth J, Gorden P, 1970 Immunoassay of plasma vasopressin in man. Proc. Natl. Acad. Sci. U. S. A 66, 1298–1305. [PubMed: 5273455]

Sahoo SK, Labhasetwar V, 2005 Enhanced antiproliferative activity of transferrin-conjugated paclitaxel-loaded nanoparticles is mediated via sustained intracellular drug retention. Mol. Pharm 2, 373–383. [PubMed: 16196490]

Sikorski EE, Hallmann R, Berg EL, Butcher EC, 1993 The Peyer’s patch high endothelial receptor for lymphocytes, the mucosal vascular addressin, is induced on a murine endothelial cell line by tumor necrosis factor-alpha and IL-1. J. Immunol (151), 5239–5250. [PubMed: 7693807]

Srinivasan B, Kolli AR, Esch MB, Abaci HE, Shuler ML, Hickman JJ, 2015 TEER measurement techniques for in vitro barrier model systems. J. Lab. Autom 20, 107–126. [PubMed: 25586998]

Striepens N, Kendrick KM, Hanking V, Landgraf R, Wullner U, Maier W, Hurlemann R, 2013 Elevated cerebrospinal fluid and blood concentrations of oxytocin following its intranasal administration in humans. Sci. Rep 3, 3440. [PubMed: 24310737]

Sundaram S, Roy SK, Ambati BK, Kompella UB, 2009 Surface-functionalized nanoparticles for targeted gene delivery across nasal respiratory epithelium. FASEB J. 23, 3752–3765. [PubMed: 19608628]

Terryn S, Francart A, Lamoral S, Hultberg A, Rommelaere H, Wittelsberger A, Callewaert F, Stohr T, Meerschaert K, Ottevaere I, Stortelers C, Vanlandschoot P, Kalai M, Van Gucht S, 2014 Protective effect of different anti-rabies virus VHH constructs against rabies disease in mice. PLoS One 9, e109367. [PubMed: 25347556]

Thompson MR, Callaghan PD, Hunt GE, Cornish JL, McGregor IS, 2007 A role for oxytocin and 5-HT(1A) receptors in the prosocial effects of 3,4 methylenedioxymethamphetamine (“ecstasy”). Neuroscience 146, 509–514. [PubMed: 17383105]

Tong W, Wang L, D’Souza MJ, 2003 Evaluation of PLGA microspheres as delivery system for antitumor agent-camptothecin. Drug Dev. Ind. Pharm 29, 745–756. [PubMed: 12906332]

Tukey JW, 1949 Comparing individual means in the analysis of variance. Biometrics 5, 99–114. [PubMed: 18151955]

Ulbrich K, Hekmatara T, Herbert E, Kreuter J, 2009 Transferrin- and transferrinreceptor-antibody-modified nanoparticles enable drug delivery across the blood-brain barrier (BBB). Eur. J. Pharm. Biopharm 71, 251–256. [PubMed: 18805484]

Watanabe T, Dohgu S, Takata F, Nishioku T, Nakashima A, Futagami K, Yamauchi A, Kataoka Y, 2013 Paracellular barrier and tight junction protein expression in the immortalized brain

endothelial cell lines bEND.3, bEND.5 and mouse brain endothelial cell 4. Biol. Pharm. Bull 36, 492–495. [PubMed: 23449334]

Wiley DT, Webster P, Gale A, Davis ME, 2013 Transcytosis and brain uptake of transferrin-containing nanoparticles by tuning avidity to transferrin receptor. Proc. Natl. Acad. Sci. U. S. A 110, 8662–8667. [PubMed: 23650374]

Williams RL, Courtneidge SA, Wagner EF, 1988 Embryonic lethalities and endothelial tumors in chimeric mice expressing polyoma virus middle T oncogene. Cell 52, 121–131. [PubMed: 3345558]

Woldbye DP, 1998 Antiepileptic effects of NPY on pentylenetetrazole seizures. Regul. Pept 75–76, 279–282.

Wuest DM, Wing AM, Lee KH, 2013 Membrane configuration optimization for a murine in vitro blood-brain barrier model. J. Neurosci. Methods 212, 211–221. [PubMed: 23131353]

Yan F, Wang Y, He S, Ku S, Gu W, Ye L, 2013 Transferrin-conjugated, fluorescein-loaded magnetic nanoparticles for targeted delivery across the blood-brain barrier. J. Mater. Sci. Mater. Med 24, 2371–2379. [PubMed: 23793566]

Ying X, Wen H, Lu WL, Du J, Guo J, Tian W, Men Y, Zhang Y, Li RJ, Yang TY, Shang DW, Lou JN, Zhang LR, Zhang Q, 2010 Dual-targeting daunorubicin liposomes improve the therapeutic efficacy of brain glioma in animals. J. Control. Release 141, 183–192. [PubMed: 19799948]

Zaman RU, Mulla NS, Braz Gomes K, D'Souza C, Murnane KS, D'Souza MJ, 2018 Nanoparticle formulations that allow for sustained delivery and brain targeting of the neuropeptide oxytocin. Int. J. Pharm 548, 698–706. [PubMed: 30031864]

Zhang X, Koh CG, Yu B, Liu S, Piao L, Marcucci G, Lee RJ, Lee LJ, 2009 Transferrin receptor targeted lipopolyplexes for delivery of antisense oligonucleotide g3139 in a murine k562 xenograft model. Pharm. Res 26, 1516–1524. [PubMed: 19291371]

Zoicas I, Slattery DA, Neumann ID, 2014 Brain oxytocin in social fear conditioning and its extinction: involvement of the lateral septum. Neuropsychopharmacology 39, 3027–3035. [PubMed: 24964815]

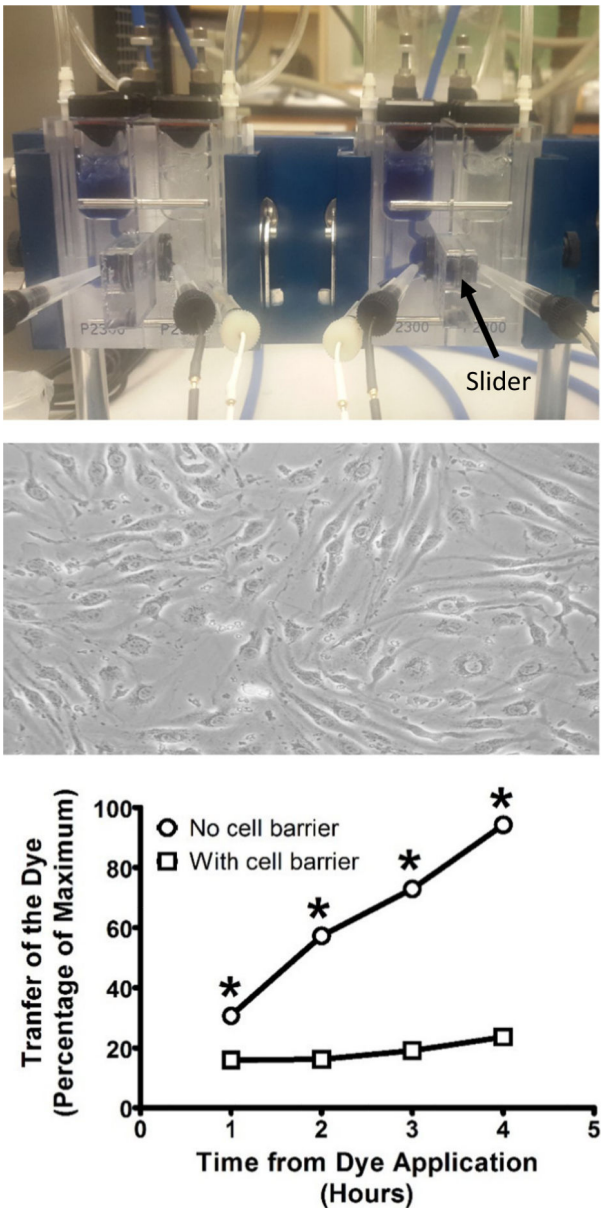

Fig. 1.

Validation studies to determine the integrity of the artificial blood-brain barrier formed by BEND3 cells. TOP: Representative picture of a double setup Ussing chamber for the measurement of transepithelial electrical resistance and macromolecular transport. MIDDLE: Representative photomicrograph of monolayer and tight junction formation by BEND3 cells. BOTTOM: Barrier integrity was confirmed by examining transfer of trypan blue dye across the membrane using spectrophotometry at 540 nm. All points represent the mean ± SEM, and any points without error bars indicate instances in which the SEM is encompassed by the data point. *Abscissae*: Hours following the introduction of the trypan blue dye to the left compartment of the Ussing chamber. *Ordinates*: Percentage of the dye that crossed to the right side of the Ussing chamber normalized to the amount remaining on

the left side. All assessments were conducted in triplicate. * = $p < 0.05$ in comparison to the presence of the cellular barrier.

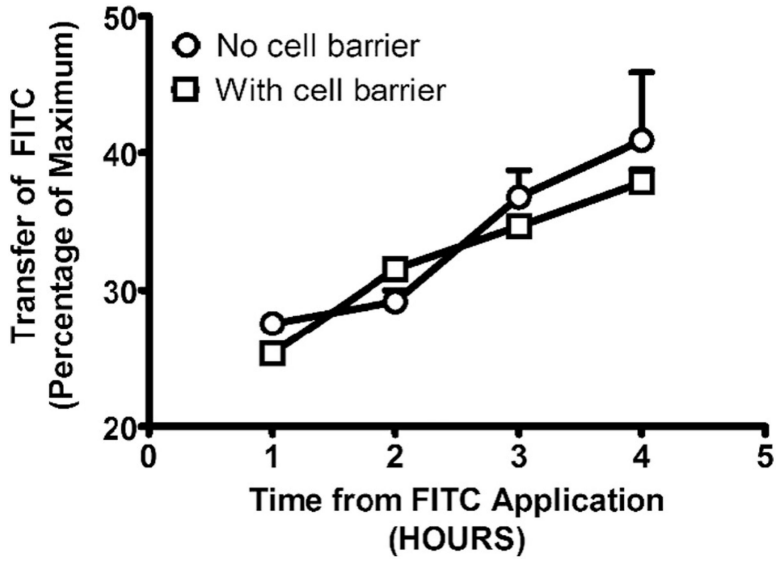

Fig. 2.

Transport of fluorescein isothiocyanate (FITC) encapsulated in Tf-coated nanoparticles across the artificial blood-brain barrier formed by BEND3 cells. The extent of transport was assessed by quantifying the fluorescence intensity of FITC using a fluorescent spectrophotometer at an excitation wavelength of 485 nm and an emission wavelength of 528 nm. All points represent the mean ± SEM, and any points without error bars indicate instances in which the SEM is encompassed by the data point. *Abscissae*: Hours following the introduction of the FITC dye to the left compartment of the Ussing chamber. *Ordinates*: Percentage of FITC that crossed to the right side of the Ussing chamber normalized to the amount remaining on the left side. All assessments were conducted in triplicate.

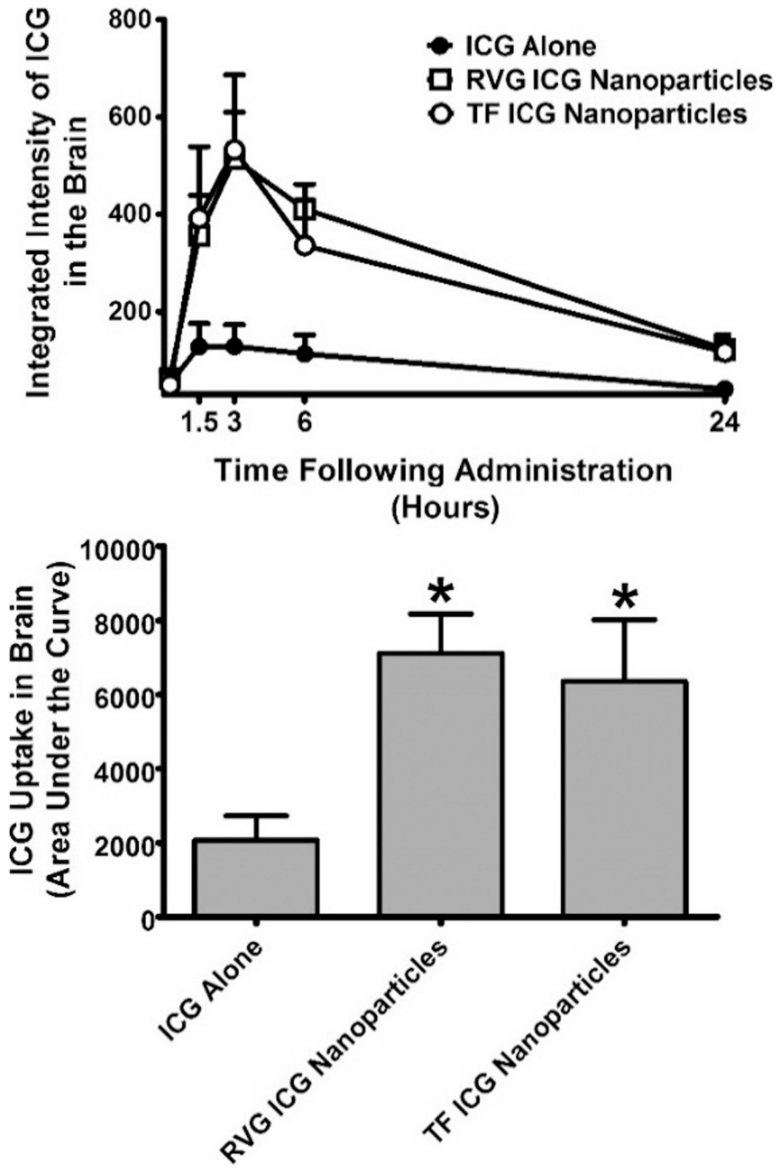

Fig. 3.

Extent of uptake Indocyanine green (ICG) dye in the brain when given alone or in either transferrin (Tf) or rabies virus glycoprotein (RVG)-coated nanoparticles through intranasal administration in Swiss-Webster mice. The integrated intensity of the dye in the brain was determined using a LI-COR Odyssey bioimager at 800 nm. TOP: Time course of ICG uptake in brain. BOTTOM: Area under the curve determined across the individual mice. All points represent the mean ± SEM, and any points without error bars indicate instances in which the SEM is encompassed by the data point. *Abscissae*: Hours following intranasal administration of ICG (top) or treatment condition (bottom). *Ordinates*: Integrated uptake of ICG in brain expressed in raw values (top) or as the area under the curve (bottom). All assessments were conducted in triplicate. * = $p < 0.05$ as assessed by one-way analysis of variance and Dunnett's post-hoc test in comparison to ICG alone.

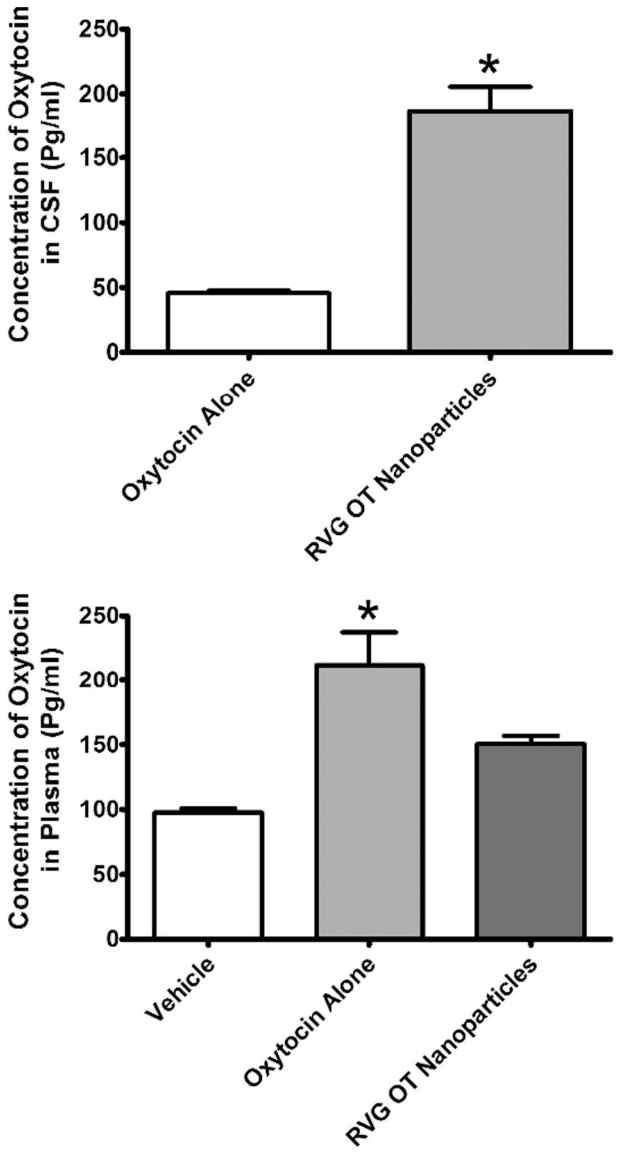

Fig. 4.

Concentration of oxytocin (OT) in cerebrospinal fluid (CSF) or plasma 2 h after intranasal administration of vehicle, OT alone, or OT encapsulated in rabies virus glycoprotein (RVG)-coated nanoparticles. Levels of OT in CSF following vehicle administration are not shown as they were below the limit of detection. TOP: Concentration of OT in the CSF. BOTTOM: Concentration of OT in the CSF. OT levels were determined in CSF and plasma by ELISA. *Abscissae*: Treatment condition. *Ordinates*: Concentration of OT in CSF (top) or plasma (bottom). All assessments were conducted in duplicate. * = $p < 0.05$ as assessed by unpaired *t*-test.

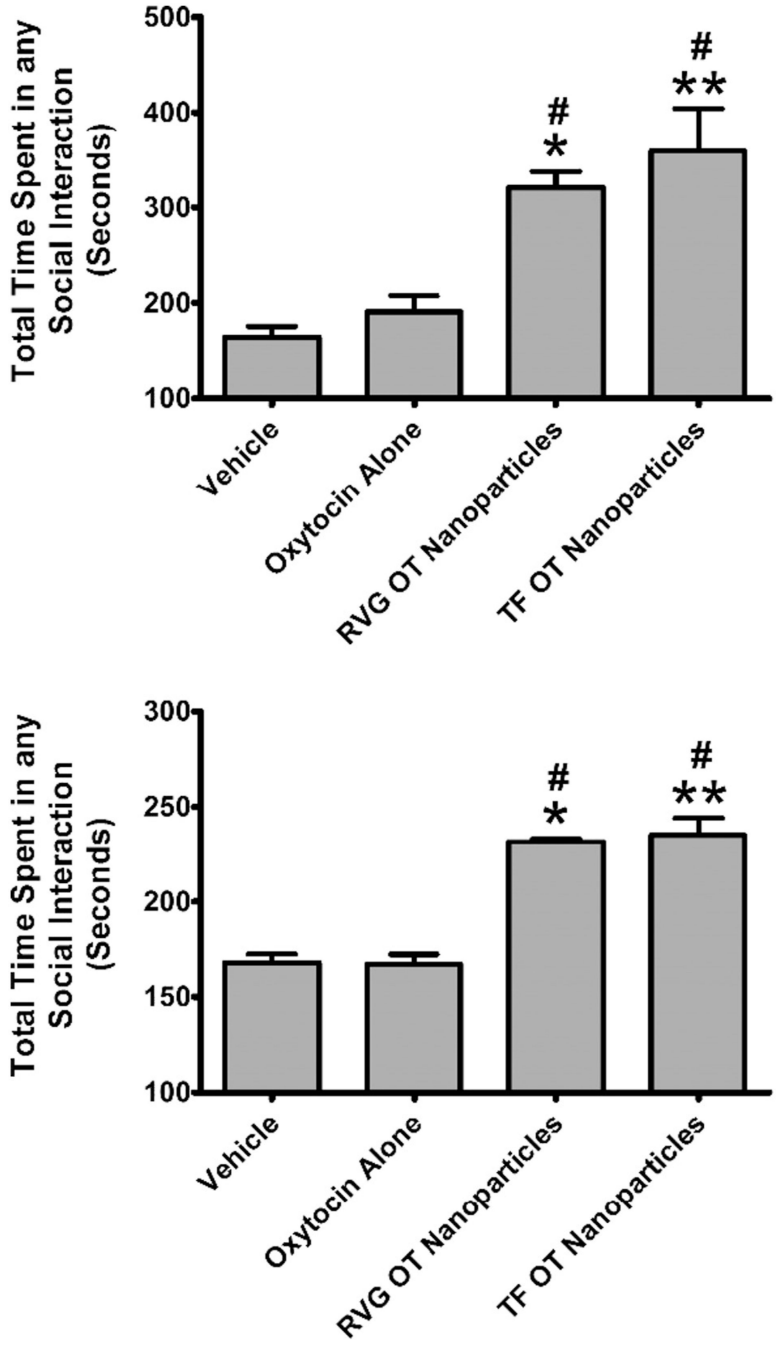

Fig. 5.

Dyadic social interactions following delivery of oxytocin (OT) alone or in either transferrin (Tf) or rabies virus glycoprotein (RVG)-coated nanoparticles through intranasal administration in Swiss-Webster mice. Social interactions were assessed over a period of 10 min and were observationally scored using 6-point scale. TOP: Social behavior assessed 2 h after OT administration. BOTTOM: Social behavior assessed 3 days after OT administration using identical procedures to the acute test (including 120 min of separation). *Abscissae*: Treatment condition. *Ordinates*: Time in seconds spent in any social interaction. * = $p < 0.05$

compared to vehicle; ** = $p < 0.01$ compared to vehicle; # = $p < 0.05$ compared to oxytocin alone as assessed by one-way analysis of variance and Tukey's post-hoc test.

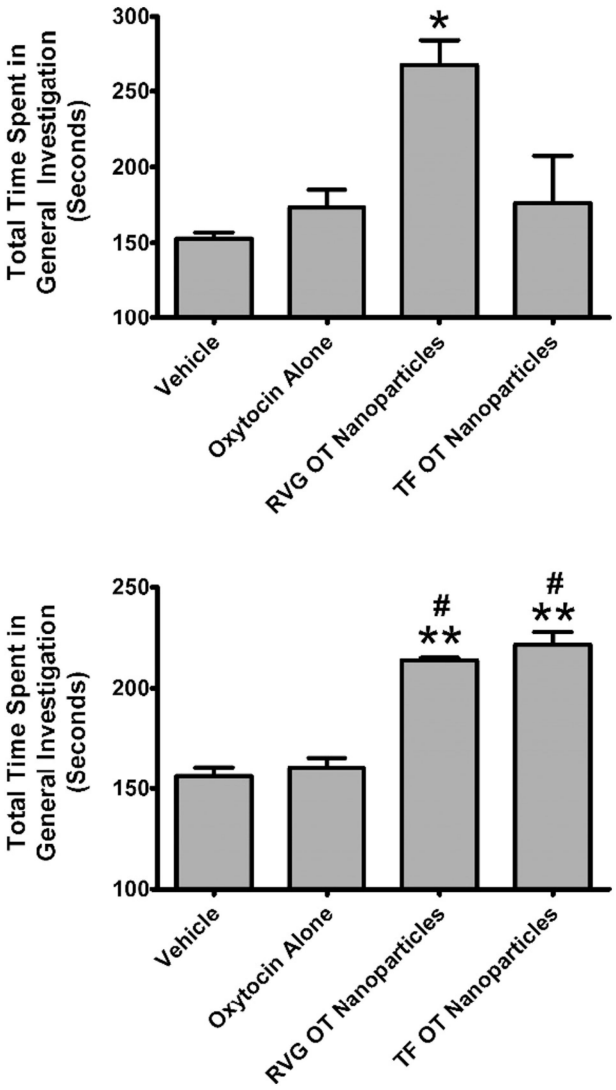

Fig. 6.

Assessment of the general investigation component of dyadic social interactions following delivery of oxytocin (OT) alone or in either transferrin (Tf)- or rabies virus glycoprotein (RVG)-coated nanoparticles through intranasal administration in Swiss-Webster mice. TOP: Social behavior assessed 2 h after OT administration. BOTTOM: Social behavior assessed 3 days after OT administration using identical procedures to the acute test (including 120 min of separation). *Abscissae*: Treatment condition. *Ordinates*: Time in seconds spent in general investigation. * = $p < 0.05$ compared to vehicle; ** = $p < 0.01$ compared to vehicle; # = $p < 0.05$ compared to oxytocin alone as assessed by one-way analysis of variance and Tukey's post-hoc test.